nature plants

ARTICLES

PUBLISHED: 31 OCTOBER 2016 | ARTICLE NUMBER: 16169 | DOI: 10.1038/NPLANTS.2016.169

The DNA demethylase ROS1 targets genomic regions with distinct chromatin modifications

Kai Tang[1†], Zhaobo Lang[1,2*†], Heng Zhang[2] and Jian-Kang Zhu[1,2]

The *Arabidopsis* ROS1/DEMETER family of 5-methylcytosine (5mC) DNA glycosylases are the first genetically characterized DNA demethylases in eukaryotes. However, the features of ROS1-targeted genomic loci are not well understood. In this study, we characterized ROS1 target loci in *Arabidopsis* Col-0 and C24 ecotypes. We found that ROS1 preferentially targets transposable elements (TEs) and intergenic regions. Compared with most TEs, ROS1-targeted TEs are closer to protein coding genes, suggesting that ROS1 may prevent DNA methylation spreading from TEs to nearby genes. ROS1-targeted TEs are specifically enriched for H3K18Ac and H3K27me3, and depleted of H3K27me and H3K9me2. Importantly, we identified thousands of previously unknown RNA-directed DNA methylation (RdDM) targets following depletion of ROS1, suggesting that ROS1 strongly antagonizes RdDM at these loci. In addition, we show that ROS1 also antagonizes RdDM-independent DNA methylation at some loci. Our results provide important insights into the genome-wide targets of ROS1 and the crosstalk between DNA methylation and ROS1-mediated active DNA demethylation.

An important epigenetic mark present in many eukaryotes, 5mC, is involved in many crucial biological processes, such as gene imprinting, regulation of gene expression and genome stability[1–3]. In plants, DNA methylation frequently occurs in three sequence contexts, including CG, CHG and CHH (H represents either A, C or T). In *Arabidopsis*, DNA methylation is established and maintained by different pathways. DNA methylation (*de novo* methylation) is established by domains rearranged methyltransferase 2 (DRM2), through the RNA-directed DNA methylation (RdDM) pathway, in which RNA polymerase IV (Pol IV)-dependent 24 nt small interfering RNAs (siRNAs) function to guide DRM2 to target loci. Recently, it was found that Pol IV-dependent 25–35 nt precursors of the 24 nt siRNAs can trigger DNA methylation independently of the 24 nt siRNAs[4–7]. Four different enzymes maintain DNA methylation after DNA replication, depending on the sequence context: mCG is maintained by DNA methyltransferase 1 (MET1), mCHG is maintained by chromomethylase3 (CMT3) and mCHH is maintained by CMT2 and DRM2.

DNA methylation levels are dynamically regulated. DNA methylation can be passively lost because of lack of maintenance methylation, or can be actively removed by DNA demethylases[3]. In plants, active DNA demethylation is initiated by the ROS1/Demeter family of proteins. ROS1 is the first genetically characterized DNA demethylase (the first enzyme in the active DNA demethylation pathway) in eukaryotes[8]. ROS1 can remove the 5mC base and nick the DNA backbone, leaving a single nucleotide gap that is filled with an unmethylated cytosine through a base excision repair pathway[9–13]. An anti-silencing protein complex containing methyl-DNA binding protein 7 (MBD7), increased DNA methylation 1 (IDM1), IDM2 and IDM3, was recently discovered to regulate ROS1 targeting and, in turn, DNA demethylation[14–16]. In *Arabidopsis*, some TEs show lower expression levels in *ros1* mutants because of increased DNA methylation[15,17]. Some genes are silenced in *ros1* mutants because of DNA hypermethylation of nearby TEs[14,17–19], suggesting that ROS1-mediated demethylation of TEs is important for regulation of gene expression by preventing nearby genes from being silenced. The methylomes of an *Arabidopsis ros1/dml2/dml3* (*rdd*) triple mutant[20] and of a *ros1* single mutant[14] have been analysed, revealing thousands of genomic regions subjected to active DNA demethylation by ROS1[14]. However, the features of ROS1 targets are not known.

Previous studies suggested interactions between ROS1-mediated DNA demethylation and RdDM[21–23]. Recently, studies revealed that the expression of *ROS1* is finely tuned by RdDM and DNA demethylation pathways[24,25], although the genome-wide interaction between ROS1-mediated DNA demethylation and RdDM has not been investigated. In this study, we generated and analysed the DNA methylomes of *ros1* mutants in both Col-0 and C24 ecotypes of *Arabidopsis*, and characterized ROS1 target loci in these two genetic backgrounds. Our analyses identified and characterized thousands of genomic loci that are regulated by both ROS1 and RdDM. Interestingly, we discovered thousands of previously unidentified RdDM targets by analysing the DNA methylome of *ros1/nrpd1* double mutant plants that are defective in both active DNA demethylation and RdDM. In addition, we show that besides antagonizing RdDM, ROS1 can also antagonize RdDM-independent DNA methylation at more than a thousand genomic loci. These results provide important insights into the genome-wide effect of ROS1-mediated active DNA demethylation and the interaction between DNA demethylation and methylation in plants.

Results

Characterization of *ros1* mutant methylomes in Col-0 and C24 ecotypes. *ros1-4* is an *Arabidopsis* mutant of Col-0 ecotype with T-DNA insertion in the *ROS1* gene causing complete loss of function of *ROS1* (ref. 26). *ros1-1* is a loss-of-function mutant of ROS1 in C24 ecotype and has a single nucleotide substitution in *ROS1* leading to a premature stop codon, and is likely to be a null allele[8]. In this study, we generated single-base resolution maps of DNA methylomes of 2-week-old seedlings of *ros1-4* and *ros1-1* mutants. Methylomes of Col-0 and C24 wild types at the same developmental stage were sequenced and served as controls.

[1]Department of Horticulture and Landscape Architecture, Purdue University, West Lafayette, Indiana 47907, USA. [2]Shanghai Centre for Plant Stress Biology, and Centre for Excellence in Molecular Plant Sciences, Chinese Academy of Sciences, Shanghai 201602, China. [†]These authors contributed equally to this work. *e-mail: zblang@sibs.ac.cn

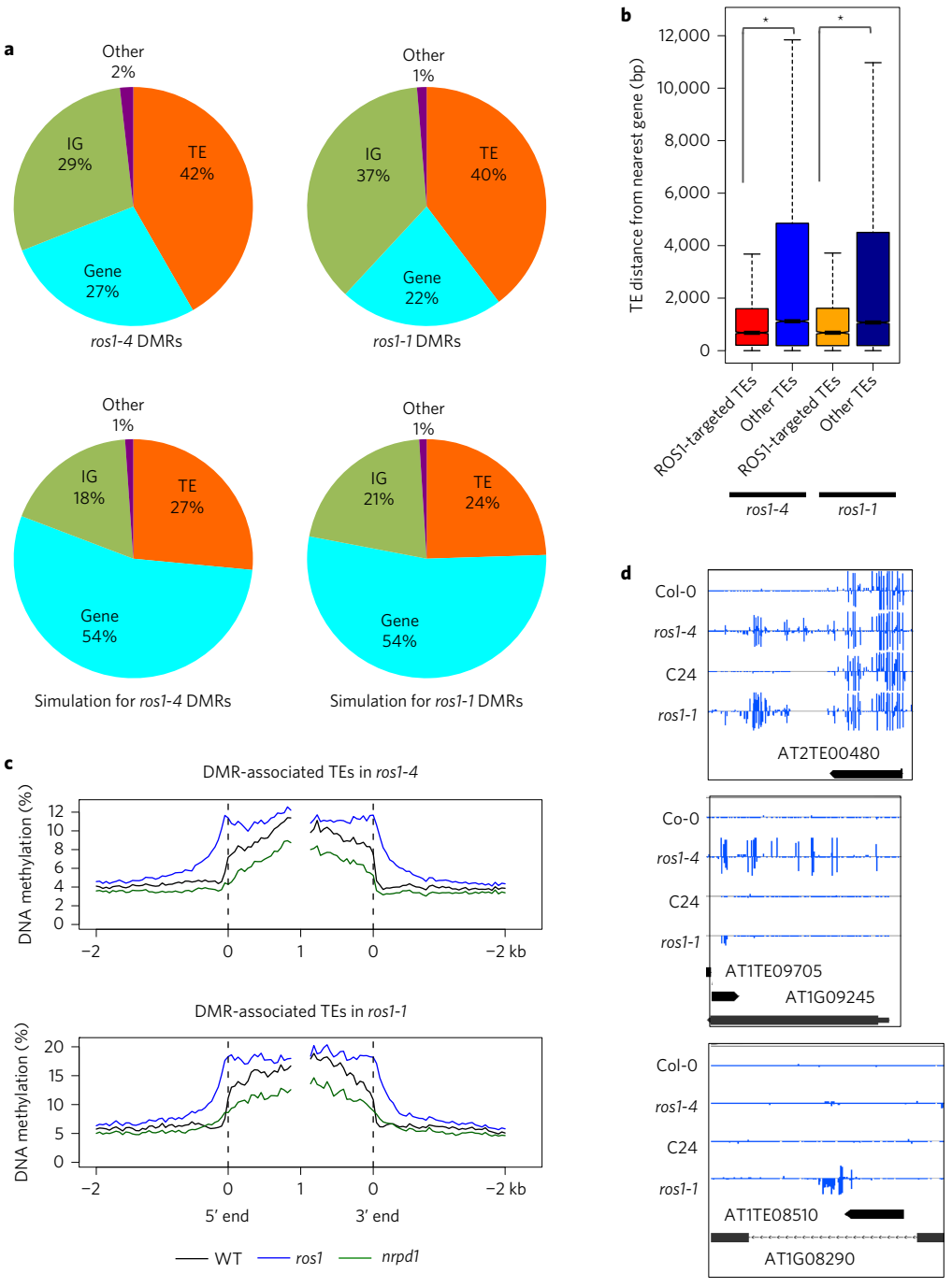

Figure 1 | Characterization of the DNA methylomes of *ros1* mutants in Col-0 and C24 ecotypes. a, The compositions of the hyper-DMRs in *ros1-4* and *ros1-1*, and of the corresponding simulated genomic regions. **b**, A box plot showing the distances between ROS1-targeted or non-targeted TEs and their nearest protein coding genes ($^*P < 2.2 \times 10^{-16}$, one-tailed Wilcoxon rank sum test). **c**, DNA methylation levels of *ros1* hyper-DMR-associated TEs in the wild type and *ros1* and *nrpd1* mutants. TEs were aligned at the 5′ end or the 3′ end, and the average methylation for all cytosines within each 50 bp interval was plotted. **d**, Methylation levels at shared or non-shared hyper-DMRs between *ros1-1* and *ros1-4*. An integrated genome browser (IGB) display of whole-genome bisulphite sequencing data is shown in the screenshots. DNA methylation levels of cytosines are indicated by the heights of vertical bars on each track.

To identify potential genomic targets of ROS1 and compare the targets in different ecotypes, we identified differentially methylated regions (DMRs) in *ros1-4* and *ros1-1* mutants relative to their respective wild type plants. *ros1-4* has 6902 hypermethylated DMRs (hyper-DMRs) with an average length of 495 bp, and 1,469 hypomethylated DMRs (hypo-DMRs) with an average length of 193 bp, and 5,011 hyper-DMRs and 332 hypo-DMRs were identified in *ros1-1*. The overwhelmingly higher numbers of hyper-DMRs than hypo-DMRs of *ros1* mutants in both Col-0 and C24 are consistent with the ROS1 function in DNA demethylation. In *ros1-4*, 1,887(27%) hyper-DMRs are in genic regions, 2,878(42%) in TE regions, 2010 (29%) in intergenic (IG) regions and 127 (2%) in the 'others' category (Fig. 1a). Compared with the composition of randomly selected control regions that are composed of 27% TEs, 54% genes and 18% IG regions (Fig. 1a), *ros1-4* hyper-DMRs have a decreased percentage in genes and increased percentages in TEs and IG regions, which is also observed in *ros1-1* hyper-DMRs (Fig. 1a). This indicates that ROS1 preferentially targets TEs and IG regions. *ros1-1* and *ros1-4*

hyper-DMRs are distributed throughout the five chromosomes of *Arabidopsis* (Supplementary Fig. 1a). For both *ros1-1* and *ros1-4* hyper-DMRs, DNA hypermethylation was detected in all three contexts (CG, CHG and CHH) (Supplementary Fig. 1b). The length distribution of ROS1 targeted TEs is similar to that of all TEs (Supplementary Table 1), suggesting that ROS1 has no preference for short or long TEs. Interestingly, by analysing the distance between TEs and its nearest genes, we found that ROS1-targeted TEs in both *ros1-1* and *ros1-4* tend to be located closer to genes relative to TEs that are not targeted by ROS1 (Fig. 1b).

In both *ros1-1* and *ros1-4*, DNA methylation is substantially increased around the boarders of TEs targeted by ROS1 (Fig. 1c). As expected, these TEs display decreased methylation in *nrpd1* mutants, which are dysfunctional for RdDM because of disruption of NRPD1, the largest subunit of RNA polymerase IV (Fig. 1c). Interestingly, we noticed that the hypermethylation in *ros1* mutants extends from the TE borders to neighbouring sequences before tempering off (Fig. 1c). These patterns support our previous hypothesis that ROS1 may counteract RdDM to prevent the spreading of methylation from highly methylated regions, such as TEs, to nearby genes[3].

To investigate the influence of different genetic backgrounds on ROS1 targeting, we compared DMRs of *ros1-4* and *ros1-1*, which are mutants in Col-0 and C24 ecotypes respectively. We found that only 27% hyper-DMRs in *ros1-4* are also hyper-DMRs in *ros1-1*, suggesting that ROS1 targeting is greatly influenced by genetic backgrounds. Interestingly, 35% of TE-type and 28% of intergenic-type hyper-DMRs are shared between *ros1-4* and *ros1-1*, but only 15% of genic type hyper-DMRs are shared between the two mutants. Thus, ROS1 targeting seems relatively conserved in TE regions in Col-0 and C24 ecotypes. Since TEs and genes typically display similar levels of genetic variation, these findings suggest that chromatin features important for active DNA demethylation might be more conserved at TEs than genes between the two ecotypes. Several examples of shared hyper-DMRs and non-shared hyper-DMRs are displayed in Fig. 1d and Supplementary Fig. 1c.

In summary, we identified, characterized, and compared targets of ROS1 in Col-0 and C24 genetic backgrounds. ROS1 targets in both Col-0 and C24 display a preference for TEs and intergenic regions, and the targeted TEs are located near genes. However, the specific genomic regions targeted by ROS1 are mostly distinct in Col-0 and C24 backgrounds.

Chromatin features associated with ROS1 targets. Histone modifications, such as histone methylation and acetylation, are known to interact with DNA methylation; therefore, we determined which histone marks are associated with ROS1 targets. Compared with simulated regions, which are randomly selected genomic regions with the same length distribution as the DMRs, both total TEs and ROS1 hyper-DMRs show a slight decrease in the level of H3 (Supplementary Fig. 2a–c), indicating a lower nucleosome density in TEs and ROS1 targets. ROS1 targets are negatively associated with most active histone marks compared with control regions, such as H3K36 di-/tri-methylation (H3K36me2/3), H3K4me2/3 and H3K9 acetylation (H3K9Ac) (Supplementary Fig. 2a–c), which was expected since a large proportion of ROS1 targets are within TEs (Fig. 1a). However, in contrast with most TEs, ROS1 targets are positively associated with the active histone mark H3K18Ac compared with control regions (Fig. 2a–c). Because only 42% of *ros1-4* hyper-DMRs are within TE regions (Fig. 1a), it is possible that the remaining 58% of *ros1* targets that are not within TEs account for the enrichment of H3K18Ac. To investigate this possibility, we compared TE, intergenic and genic types of *ros1* DMRs with simulated TEs, intergenic regions and genic regions, respectively. Consistently, we found that H3K18Ac is enriched in all types of *ros1* DMRs (Supplementary Fig. 2d), suggesting that *ros1* targets are indeed generally characterized by enrichment of H3K18Ac. The association with H3K18Ac is fully consistent with our previous finding that IDM1, an H3K18/23 acetyltransferase, is required for the demethylation of a subset of ROS1 targets[14].

We identified additional histone marks that distinguish ROS1 target regions. As shown in Fig. 2, TEs in general are negatively associated with H3K27me3, and are positively associated with H3K27me and H3K9me2. In contrast, *ros1* DMRs have the opposite features, in that they are associated with enrichment of H3K27me3 and depletion of H3K27me and H3K9me2 (Fig. 2a–c). Similarly, we compared these chromatin features of *ros1* targets and corresponding simulation for each type of regions (TE, intergenic and genic regions). All types of *ros1* targets are enriched of H3K27me3 compared with their respective simulated regions (Supplementary Fig. 2d). TE-type *ros1* targets have decreased H3K27me and H3K9me2 ChIP signals compared with the corresponding simulated regions (Supplementary Fig. 2d). We did not observe decreased H3K27me and H3K9me2 signals for genic and intergenic *ros1* targets, since the levels of these histone marks are already very low in simulated genic and intergenic regions (Supplementary Fig. 2d). These results support that *ros1* targets are associated with enrichment of H3K27me3 and depletion of H3K27me and H3K9me2.

A new class of RdDM targets. *De novo* DNA methylation, especially in the CHH context, is established through the RdDM pathway, which requires DNA-dependent RNA polymerase IV for small RNA production[27]. In previous studies, RdDM targets have been identified through the identification of hypo-DMRs in RdDM mutants compared with wild-type plants. In this study, we identified 4,580 hypo-DMRs and 2,348 hyper-DMRs in *nrpd1* (Pol IV largest subunit) mutant compared with wild-type plants; the large number of hypo-DMRs in the Pol IV mutant is consistent with the role of Pol IV in DNA methylation. The more than 2,000 hyper-DMRs in Pol IV may be related to reduced expression level of *ROS1* in *nrpd1* mutant[24,25] (see below).

Homeostasis of DNA methylation is regulated by DNA methylation and active DNA demethylation processes[3,28]. As diagrammed in Fig. 3a, regions identified as hypo-DMRs ('type I') in Pol IV mutants must be methylated in the wild type. The presence of methylation in the wild type implies that RdDM dominates active DNA demethylation at these loci or that active DNA demethylation does not occur at these loci. We refer to the 4,580 hypo-DMRs in Pol IV mutant as type I RdDM targets.

We hypothesized that DNA demethylation may be dominant over RdDM at some genomic loci. These RdDM targets ('type II') would not be methylated in wild-type plants because of the dominance of active DNA demethylation (Fig. 3a). To uncover type II RdDM targets, we introduced the *nrpd1* mutation into the *ros1-4* mutant, and compared the methylome of the *ros1/nrpd1* double mutant with that of the *ros1-4* mutant (Fig. 3a,b). The type II regions would be predicted to gain cytosine methylation in *ros1-4* mutants due to loss of *ROS1* function, however, this gained cytosine methylation would be lost in *ros1/nrpd1* mutant because of the dysfunction in RdDM. In total, we identified 6,069 hypo-DMRs in *ros1/nrpd1* compared with *ros1*. Out of the 6,069 hypo-DMRs, 3,750 display DNA methylation in wild type (mC% $\geq$ 2%), and about 60% of these 3,750 regions overlap with the 4,580 type I RdDM targets. Importantly, and consistent with our hypothesis, there are 2,319 hypo-DMRs that do not display DNA methylation in the wild type (mC% < 2%). These represent the type II RdDM targets, which have not been identified previously. Similarly, by using published methylome data of *ros1-1/nrpd1* in C24 background, we found 4,966 hypo-DMRs in *ros1-1/nrpd1* double mutant compared with *ros1-1*, and 1,656 of them are type II RdDM targets, demonstrating that type II RdDM targets exist in

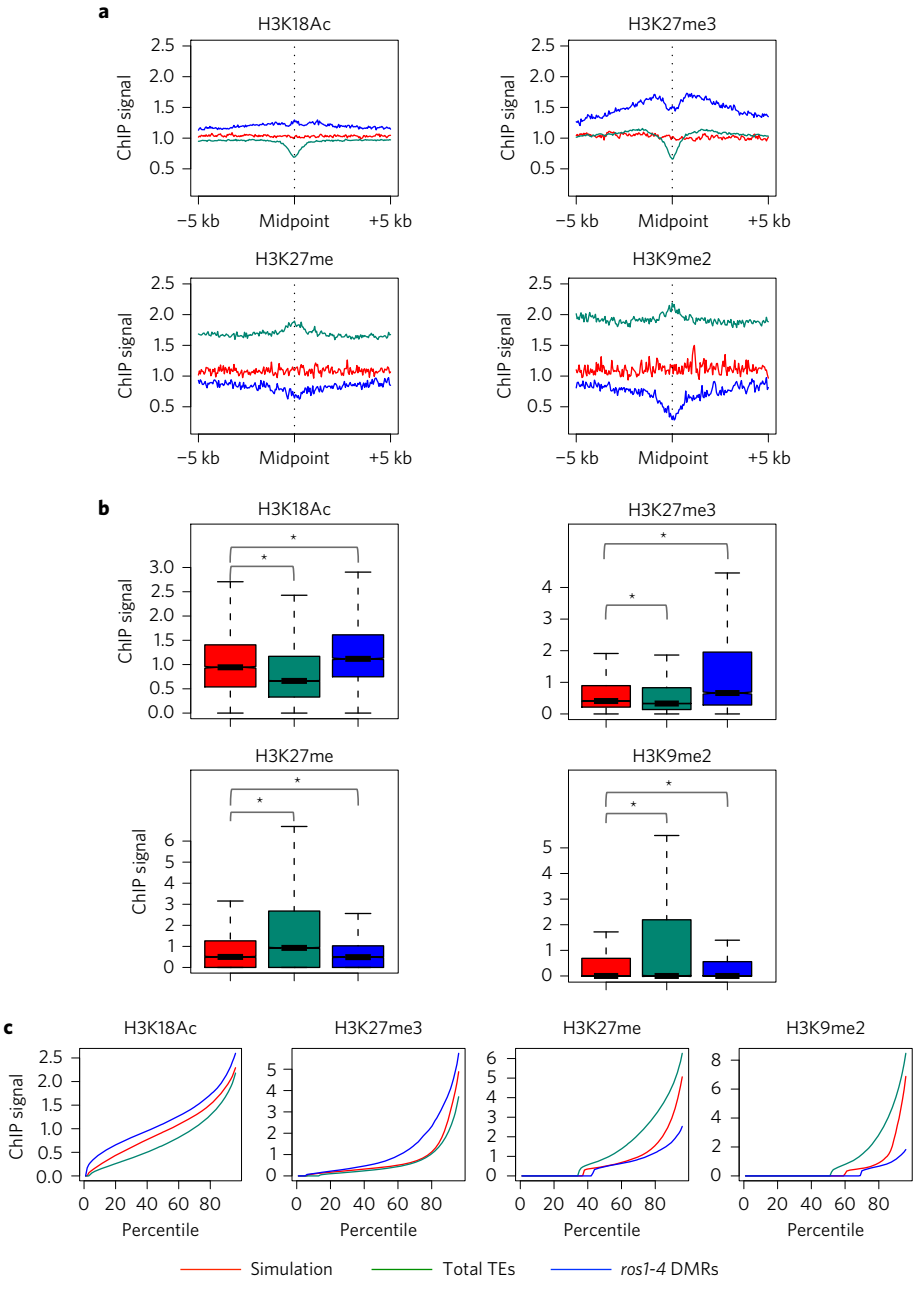

Figure 2 | Chromatin features associated with ROS1 targets. a, Association of different histone modifications surrounding *ros1-4* hyper-DMRs. Association of histone modifications at total TEs and simulated regions served as controls. In contrast to total TEs, *ros1-4* hyper-DMRs are positively associated with H3K18Ac and H3K27me3, and negatively associated with H3K27me and H3K9me2. **b**, Box plots displaying the results in **a** ($^{*}P < 1 \times 10^{-15}$, one-tailed Wilcoxon rank sum test). **c**, Percentile plots of the same data as in **b**. For each histone mark, simulated regions, TEs and *ros1-4* DMRs were ranked based on their histone ChIP signals from low (left) to high (right) along the *x* axis.

both Col-0 and C24 ecotypes. As shown in Fig. 3b,c and Supplementary Fig. 3a,b, methylation of type I loci is decreased in *nrpd1* relative to wild type. In contrast, type II loci do not display a change in methylation level in *nrpd1* (Fig. 3b,c and Supplementary Fig. 3c,d). However, introducing the *nrpd1* mutation into the *ros1-4* mutant revealed the role of RdDM in DNA methylation at the type II loci (Fig. 3a–c and Supplementary Fig. 3c,d).

We evaluated 24 nt siRNA enrichment for type II loci and found that 39% of type II loci had 24 nt siRNAs ($N > 0$ in either wild-type replicate), whereas 61% of type II loci did not display 24 nt siRNA reads ($N = 0$ in both wild-type replicates). We cannot exclude the possibility that siRNA levels at these loci were too low to be detected by siRNA-seq. Similar with type I targets, the type II targets also have a decreased siRNA level in *nrpd1* mutant relative to wild type (Supplementary Fig. 3e). This result further supports that type II loci are targets of RdDM. However, the siRNA level in type II loci is much lower than that in type I loci (Supplementary Fig. 3e), indicating weaker RdDM at type II loci.

We examined Pol IV occupancy at type I and type II loci using previously published Pol IV ChIP-seq data[29]. Pol IV is enriched in type I loci (Fig. 3d). However, we did not observe a significant enrichment of Pol IV in type II loci (Fig. 3d). The low siRNA level and low Pol IV enrichment are consistent with weak RdDM effects at these type II loci. However, type II loci display Pol IV-dependent increased DNA methylation in *ros1* mutant (Fig. 3c), suggesting enhanced RdDM at these loci in *ros1* mutant.

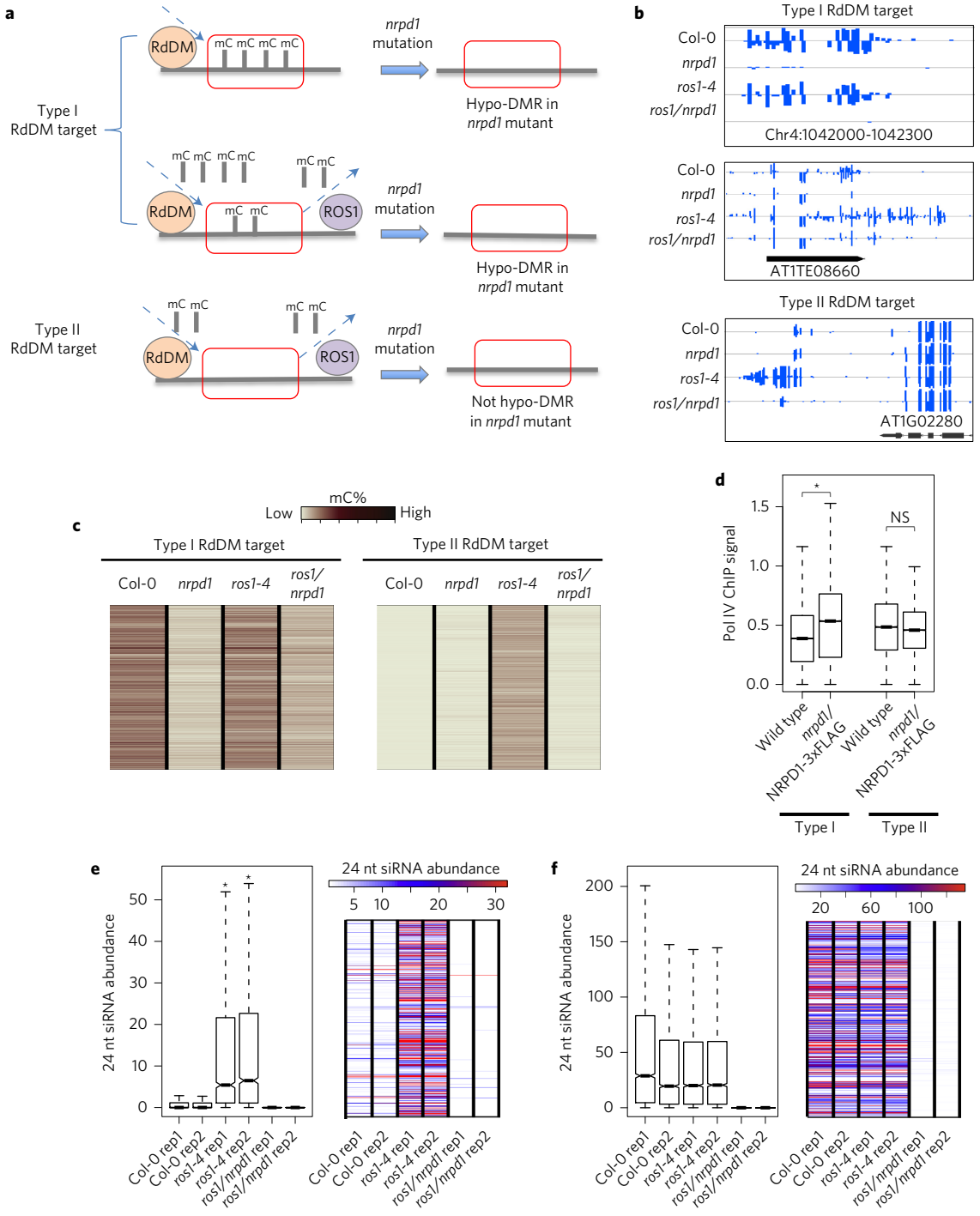

Figure 3 | Identification and characterization of type II RdDM targets. a, A schematic diagram showing the hypothesis that different RdDM targets may be regulated differently by ROS1. Some type I RdDM targets are not regulated by ROS1 (top) whereas other type I RdDM targets are, although RdDM is more dominant at these loci (middle). Type II RdDM targets are always regulated by ROS1, and ROS1 is more dominant at these loci (bottom). **b**, Methylation levels of type I and type II RdDM targets in Col-0, *nrpd1*, *ros1-4* and *ros1/nrpd1*. The three panels are representative regions as shown in **a**. **c**, Heat maps showing DNA methylation levels of all type I and type II RdDM target loci in different genotypes. **d**, A box plot showing Pol IV enrichment at type I and type II RdDM targets. The Pol IV signal in wild-type plants served as control ($^*P < 2.2 \times 10^{-16}$, one-tailed Wilcoxon rank sum test; NS, not significant). **e**, A box plot and heat map showing 24 nt siRNA abundance of type II RdDM target loci in different genotypes ($^*P < 2.2 \times 10^{-16}$, paired two-sample *t*-test). **f**, A box plot and heat map showing 24 nt siRNA abundance of type I RdDM target loci in different genotypes.

We performed small RNA-Seq in *ros1-4* mutant and *ros1-4/nrpd1* double mutant plants. We found that type II RdDM targets have a significantly elevated 24 nt siRNA level in *ros1* relative to wild-type plants, and this increase in siRNAs can be suppressed by *nrpd1* mutation (Fig. 3e). In contrast, type I RdDM targets do not display increased 24 nt siRNA levels in *ros1* mutant compared with the wild type (Fig. 3f). The results suggest that RdDM becomes stronger at type II loci when ROS1 is removed.

DRD1 is a component of the RdDM pathway, and a previous study showed that DRD1-mediated CHH methylation was positively correlated with the histone marks H3K27me3, H3K4me2, H3K4me3 and H3K36me3, and was negatively correlated with

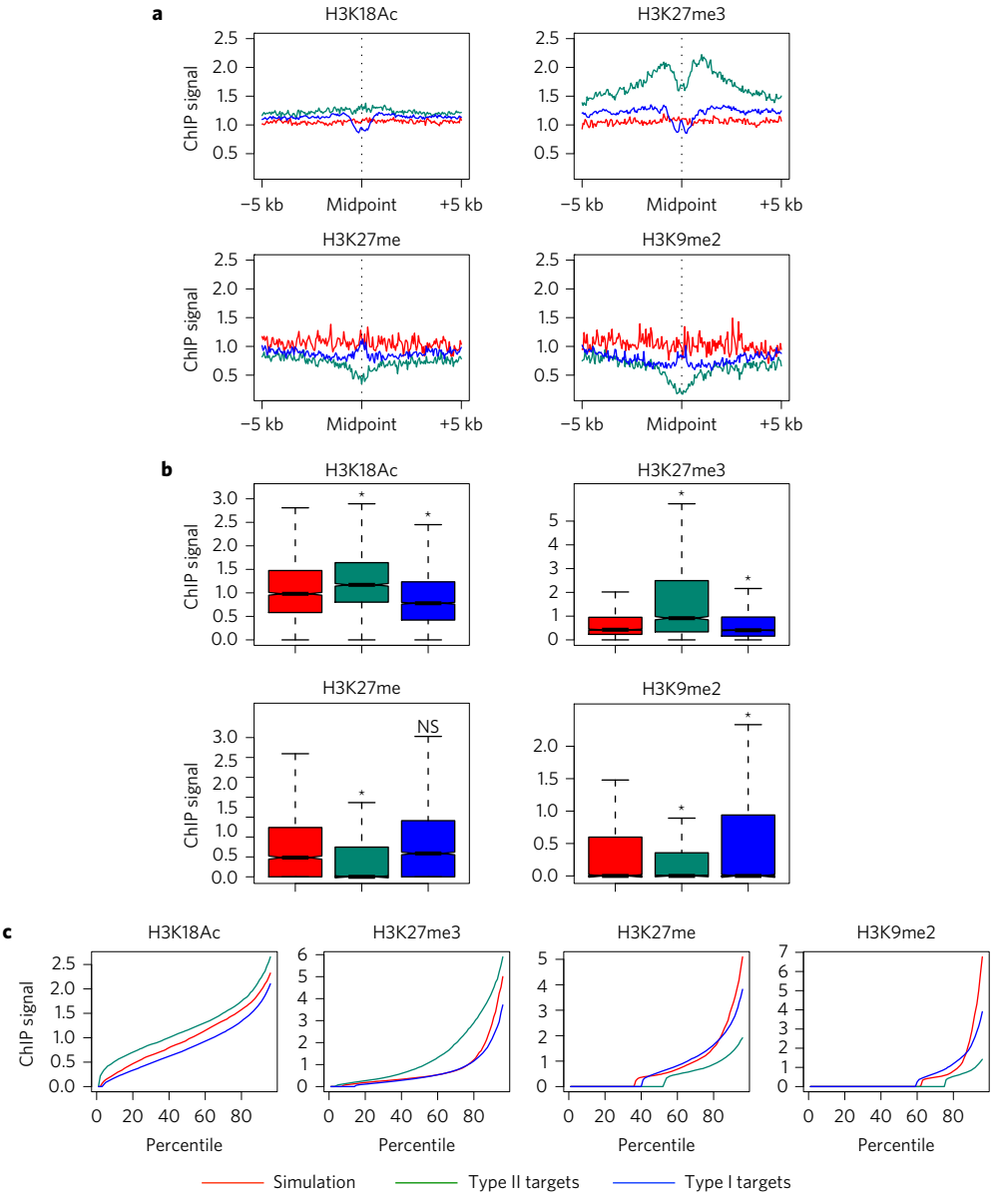

Figure 4 | Chromatin features associated with type I and type II RdDM targets. a, Association of different histone modifications at regions surrounding the mid-points of type I (blue) and type II (green) targets. Simulation regions (red) served as control regions. **b**, Box plots showing the same results as in **a** (*$P < 0.005$, one-tailed Wilcoxon rank sum test; NS, not significant compared with simulation). **c**, Percentile plots of the same data as in **b**. For each histone mark, simulated regions, type I and type II RdDM targets were ranked based on their histone ChIP signals from low (left) to high (right) along the *x* axis.

H3, H3K9me2 and H3K27me[30]. Consistent with this previous study, type I and type II RdDM targets display a slight decrease in H3 enrichment (Supplementary Fig. 4a–c), suggesting a reduced nucleosome density in RdDM target loci than in control regions. Our results show that both type I and type II targets are associated with a depletion of euchromatic histone marks, including H3K4me2/3, H3K36me2/3 and H3K9meAc (Supplementary Fig. 4a–c).

Type I and type II targets also display distinct chromatin features as shown in Fig. 4a–c. Chromatin features of type II RdDM targets are similar to ROS1 targets, including enrichment of H3K18Ac and H3K27me3 (Figs 2 and 4), as expected. In contrast, type I targets display decreased H3K18Ac and slightly decreased H3K27me3 (Fig. 4). These distinct chromatin features are supported by examination of type I and type II targets for different categories of regions (TE, intergenic and genic regions) (Supplementary Fig. 4d). Consistently, we found enrichment of H3K18Ac and H3K27me3 in all categories of type II targets compared to the corresponding categories of type I targets. Also unlike type I targets, type II targets are depleted of H3K9me2 and H3K27me. The depletion of H3K9me2 and H3K27me was found only in TE and intergenic regions of type II targets compared with type I targets, but not in genic regions of type II targets (Supplementary Fig. 4d).

In summary, type I RdDM targets show DNA methylation in the wild type, and they may or may not be regulated by ROS1. In contrast, the newly discovered type II RdDM targets are all regulated by ROS1 and are essentially depleted of DNA methylation in the wild type because of ROS1 activity. The two types of RdDM targets are also characterized by distinct small RNA profiles and histone modification marks.

Relationship between ROS1-mediated DNA demethylation and RdDM pathway. ROS1-mediated active DNA demethylation counteracts the RdDM pathway to prevent DNA hypermethylation

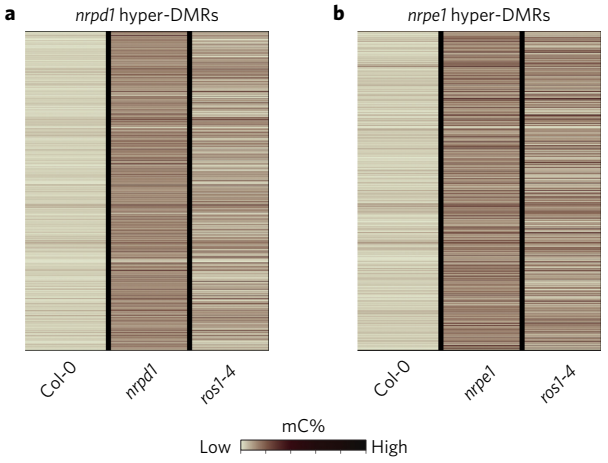

Figure 5 | Reduced *ROS1* expression contributes to DNA hypermethylation in RdDM mutants. a,**b**, Heat maps showing total C methylation levels of *nrpd1* (**a**) and *nrpe1* (**b**) hyper-DMRs in Col-0, *nrpd1* and *ros1-4*.

at some specific loci[8,31,32]. However, the genome-wide crosstalk between these two pathways has not been studied. To identify genomic regions targeted by both ROS1 and RdDM, we compared two groups of DMRs: hyper-DMRs in *ros1* mutant and hypo-DMRs in *nrpd1* mutants. We found that there are 1,136 shared DMRs between *ros1* hyper-DMRs and *nrpd1* hypo-DMRs, suggesting that 16.5% (1136/6902) of ROS1 targets are antagonized by RdDM in wild-type plants; however, this ratio increased to 60.1% (4146/6902) by using hypo-DMRs identified in *ros1/nrpd1* mutant relative to *ros1* (Supplementary Fig. 4e). These results suggest that the antagonistic effects between ROS1-mediated active DNA demethylation and RdDM have been underestimated, since type II RdDM targets were previously unappreciated.

It has been reported recently that there is a regulatory link between RdDM and ROS1-mediated active DNA demethylation. It was found that *ROS1* expression is dramatically reduced in RdDM mutants, including *nrpd1*, because of the change of DNA methylation at the promoter region of *ROS1* gene[24,25]. Thus, we speculated that the hyper-DMRs in *nrpd1* might be caused by reduced *ROS1* expression. We found that 1,026 of the 2,348 hyper-DMRs in *nrpd1* overlapped with hyper-DMRs in *ros1*, suggesting that nearly half of the hypermethylated loci in *nrpd1* might be caused by reduction of *ROS1* expression in *nrpd1*. *ROS1* expression is reduced in not only *nrpd1*, but also other RdDM mutants, such as *nrpe1* (ref. 24). As shown in Fig. 5a,b and Supplementary Fig. 5a,b, hyper-DMRs of different RdDM mutants, including *nrpd1* and *nrpe1*, also have increased DNA methylation in *ros1* mutants, suggesting that the decreased *ROS1* expression level contributes to the hypermethylation in the two examined RdDM mutants. We then determined whether the methylome of the *nrpd1* single mutant, which has a dramatically reduced *ROS1* expression level, is similar to the methylome of *ros1/nrpd1* double mutant (where *ROS1* was knocked out). After comparing *ros1/nrpd1* with *nrpd1*, we identified 3,411 hyper-DMRs in *ros1/nrpd1* relative to *nrpd1*. Interestingly, only 35% of the 3,411 hyper-DMRs are included in the 6,902 hyper-DMRs in *ros1-4*, suggesting that ROS1 may have new target loci in *nrpd1* mutant compared with those in the wild type. This finding suggests that the remaining *ROS1* expression in *nrpd1* mutants still functions at thousands of loci, although other demeter-like proteins (DMLs) may also contribute to these hyper-DMRs.

ROS1 antagonizes RdDM-independent DNA methylation. We identified 1,026 shared hypermethylated loci in *nrpd1* and *ros1* (Fig. 6a), which are distributed across five chromosomes (Supplementary Fig. 6a). Although these loci have similar chromatin features to ROS1 targets, such as H3K18Ac, H3K4me2 and H3K4me3, they display slightly increased levels of H3 compared with general ROS1 targets (Supplementary Fig. 6b). At these loci, ROS1 prevents hypermethylation, and the methylation must be independent of RdDM since the methylation can occur in *nrpd1* mutants. This indicates that there are RdDM-independent pathways responsible for the methylation and are antagonistic to ROS1 at these loci. Using previously published methylome data (Supplementary Table 2), we examined methylation levels of these 1,026 loci in wild type, *nrpd1*, *ros1*, *drm2*, *drm1drm2*, *cmt2*, *cmt3*, *cmt2cmt3*, *drm1/drm2/cmt2 (ddcmt2)*, *drm1/drm2/cmt3 (ddcmt3)*, *drm1/drm2/cmt2/cmt3 (ddcc)* and *met1* mutants. The *nrpd1*, *ros1* and *drm2* mutants display increased mCG, mCHG and mCHH levels at these loci (Fig. 6b–d), suggesting that MET1, DRM1, CMT2 and CMT3 may all contribute to the methylation at these loci. Indeed, we found that the mCG level of these loci is significantly reduced in *met1* (Fig. 6b), whereas the mCHG levels are significantly reduced in *cmt3* (Fig. 6c). Although CMT2 and CMT3 have been shown to function redundantly in mCHG methylation[33], it seems that the mCHG methylation at these loci mainly depends on CMT3 (Fig. 6c). For mCHH methylation level, there are no significant changes in *cmt2* and *cmt2cmt3* double mutants. However, mCHH is significantly reduced in *ddcmt2* and *ddcc* mutants but is increased in *drm2*, *drm1drm2* and *ddcmt3* (Fig. 6d). This indicates that DRM1 and CMT2 may function redundantly at these regions.

At these loci, mCHG and mCHH levels are increased in *met1* mutant plants (Fig. 6c,d). This may be caused by the reduction in *ROS1* expression in *met1* mutants[34], such that the mCHG and mCHH methylation by CMT3, CMT2 and DRM1 could not be removed by ROS1. These results suggested that ROS1 antagonizes CMT3-, CMT2-, DRM1- and MET1-mediated DNA methylation, which are independent of DRM2, the major DNA methyltransferase in the RdDM pathway (Supplementary Fig. 6c).

We examined siRNA levels at these 1,026 loci in wild type and *nrpd1*, and found that 24 nt siRNAs accumulate at the loci in the wild type, but are lost in *nrpd1* mutant plants (Supplementary Fig. 6d). Since the siRNAs but not DNA methylation at these loci are dependent on Pol IV, the siRNAs at these loci would not be required for the methylation. This is consistent with a recent study showing that a reduction of siRNA levels in RdDM mutants does not substantially reduce CMT2-dependent CHH methylation[33].

In summary, our study revealed that, besides RdDM, ROS1 can antagonize DNA methylation mediated by MET1, DRM1 and CMTs in an siRNA-independent manner.

Discussion

Among the four proteins in the ROS1/Demeter family in *Arabidopsis*, ROS1 is the major DNA demethylase in vegetative tissues. In this study, we showed that genome-wide, ROS1 preferentially targets TEs that are close to protein coding genes (Fig. 1b). We also showed that the sequences just outside the boarders of ROS1-targeted TEs have increased DNA methylation in *ros1* mutants (Fig. 1c), suggesting that ROS1 prevents the spreading of DNA methylation from highly methylated TEs. Consistently, Yamamuro *et al.*[18] reported that ROS1 is required for the expression of the *EPF2* gene by preventing the spreading of methylation from a TE near the promoter of *EPF2*. In addition, ROS1 family demethylases can positively regulate fungal pathogen responsive genes via demethylating TEs located in or near their promoters[19]. Together with these previous studies, our data support that ROS1 is involved in the regulation of gene expression by preventing DNA methylation spreading from nearby TEs.

H3K18Ac is an active histone mark correlated with transcriptional activation[35]. We found that ROS1 targets are positively associated with H3K18Ac (Fig. 2a–c), supporting our previous work

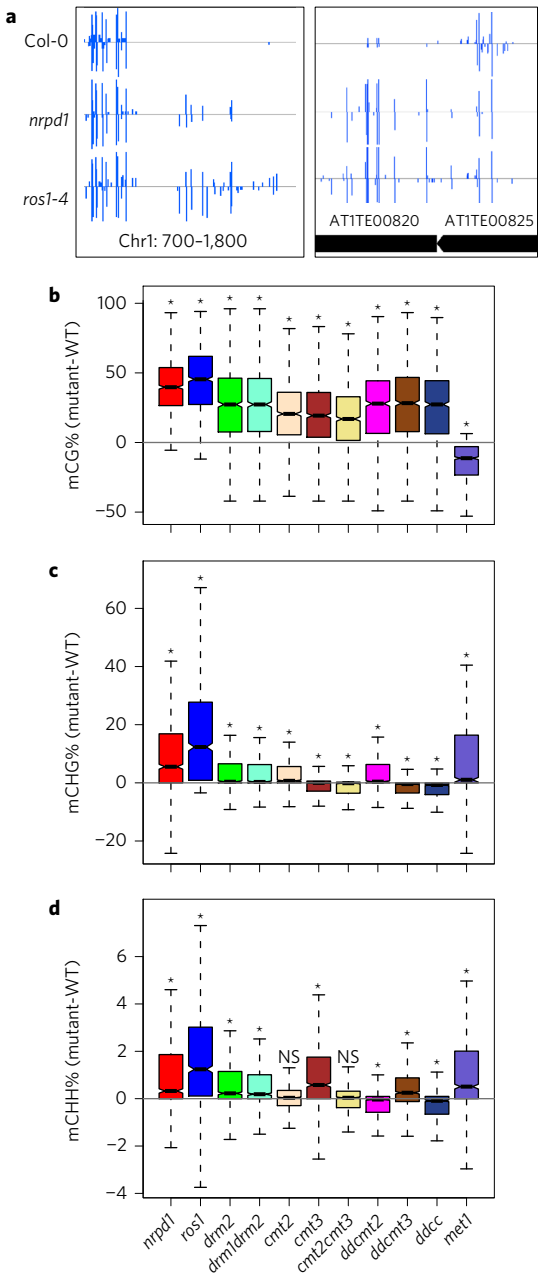

Figure 6 | ROS1 antagonizes RdDM-independent DNA methylation. a, IGB display of DNA methylation levels at shared hyper-DMRs between *nrpd1* and *ros1-4*. DNA methylation levels of cytosines are indicated by the heights of the vertical bars on each track. **b–d**. The 1,026 genomic regions with increased DNA methylation in both *ros1* and *nrpd1* mutants were used. Box plots of CG (**b**), CHG (**c**) and CHH (**d**) methylation level changes (mutant-WT) of these regions were shown in different mutants. *ddcmt2* is the *drm1drm2cmt2* triple mutant, *ddcmt3* is the *drm1drm2cmt3* triple mutant and *ddcc* is the *drm1drm2cmt2cmt3* quadruple mutant. (*$P < 1 \times 10^{-10}$, one sample one-tailed Student's *t*-test).

showing that IDM1, an H3K18/23 acetyltransferase, can create a permissive chromatin environment important for ROS1 to access target loci[14]. ROS1 targets were also found to be enriched with H3K27me3, but depleted of H3K27me and H3K9me2, in contrast to general TEs (Fig. 2a–c). This is consistent with a previous finding that there was a strong correlation between H3K18Ac and H3K27me3 in *Arabidopsis*[36], and is also consistent with findings in mammals that DNA demethylation process is coupled with decreased H3K9me2 and increased H3K27me3[37].

Consistent with previously observed antagonism between ROS1 and RdDM, ROS1-targeted TEs display decreased DNA methylation in *nrpd1* mutants (Fig. 1c). We hypothesized that ROS1-mediated DNA demethylation may be so strong at some loci that methylation does not accumulate in the wild type at these regions. These potential RdDM targets could not be identified by comparing RdDM mutants with wild-type plants; however, in this study we discovered more than 2,000 of these 'type II' RdDM targets by comparing *ros1* and *ros1/nrpd1* mutants. These RdDM targets have eluded previous attempts of RdDM target identification. Our discovery of type II loci suggests that the number of RdDM targets has been greatly underestimated.

Overall siRNA enrichment and Pol IV occupancy were lower at type II targets than type I targets. More than half of the type II loci do not have any siRNA reads, and we did not observe any significant Pol IV enrichment at type II loci. The type II loci may be better targeted by RdDM in the *ros1* mutant background. We observed increased siRNA levels at type II loci in *ros1-4* mutant, indicating that RdDM becomes stronger in *ros1* mutant plants. It is possible that demethylation or occupancy by ROS1 at these loci in wild-type plants limits RdDM accessibility, thus leading to weak RdDM in the wild type, and that this inhibition of RdDM in the wild type is alleviated by *ros1* mutation. ROS1 has been shown to have a similar binding affinity to both methylated and non-methylated DNA through a Lysine-rich Domain at the amino terminus[38]. Thus, it is possible that ROS1 antagonizes RdDM not only by removal of DNA methylation, but also by preventing the access of RdDM machinery to the target loci. In the future, it will be interesting to compare Pol IV occupancy at these loci in wild-type and *ros1* mutant plants to further investigate this possibility.

It is well known that *ROS1* expression is dramatically reduced in RdDM mutants[24]. Our results suggested that the reduction in *ROS1* expression in *nrpd1* mutant plants induces DNA hypermethylation at more than a thousand genomic regions. The DNA hypermethylation in RdDM mutants must also be caused by some RdDM-independent DNA methylation pathways. Our analysis suggested that four DNA methylases including DRM1, CMT2, CMT3 and MET1 contribute to the hypermethylation in RdDM mutants. This finding implies that ROS1 can also antagonize RdDM-independent DNA methylation. Interestingly, we noticed that the *nrpd1* mutant has slightly increased DNA methylation at type II RdDM loci compared with the wild type (Fig. 3c): 198/2319 type II loci overlap with the 1,026 hyper-DMRs in *nrpd1* mutant. Thus, RdDM-independent DNA methylation may compensate to methylate DNA at some type II loci when RdDM is lacking. Our findings suggest that the fine tuning of the plant methylome is complex and involves interactions between DNA methylation mediated by RdDM and RdDM-independent mechanisms, and DNA demethylation mediated by ROS1 family demethylases.

Methods

Plant materials. Mutants including *ros1-4*, *nrpd1-3* (SALK_128428), *ros1/nrpd1* double mutant and *nrpe1-11* (SALK_029919) are in the Col-0 background. *ros1-4* and *nrpd1-3* were crossed to generate *ros1/nrpd1* double mutant. *ros1-1*, *nrpd1(C24)* and *ros1-1/nrpd1(C24)* are mutants of C24 ecotype.

Seeds were stratified for 2–3 days at 4 °C before being sown on 1/2 MS plates containing 2% (wt/vol) sucrose and 0.7% (wt/vol) agar. All of the plants were grown under long day conditions at 22 °C.

Whole-genome bisulphite sequencing and analysis. DNA was extracted from 1 gram of 14-day-old seedlings using the Plant DNeasy Maxi Kit from Qiagen. And 5 μg of gDNA was used for library construction using Illumina's standard DNA methylation analyses protocol and the TruSeq DNA sample preparation kit. The samples in the Col-0 background were sequenced in the Genomics Core Facilities of the Shanghai Centre for Plant Stress Biology, Shanghai Institutes for Biological Sciences, Chinese Academy of Sciences (Shanghai, China) with Illumina HiSeq2500. The samples in C24 background were sequenced in the Biosciences Core Laboratory of King Abdullah University of Science & Technology (KAUST) with Illumina HiSeq2000.

For Col-0 background data analysis, low-quality sequences ($q < 20$) were trimmed using trim in BRAT-BW (ref. 39), and clean reads were mapped to the TAIR10 genome using BRAT-BW and allowing two mismatches. To remove potential PCR duplicates, the remove-dupl command of BRAT-BW was used. DMRs were identified according to Ausin *et al.*[40] with minor modification. In brief, only cytosines with 4× coverage in all libraries in the same background were considered. A sliding-window approach with a 200 bp window sliding at 50 bp intervals was used to identify DMRs. Fisher's exact test was performed for methylated versus unmethylated cytosines for each context, within each window, with false discovery rates (FDRs) estimated using a Benjamini–Hochberg adjustment of Fisher's *P*-values calculated in the R environment. Windows with an FDR ≤ 0.05 were considered for further analysis, and windows within 100 bp of each other were merged to larger regions. Regions were then adjusted to shrink to the first and last differentially methylated cytosines (DMCs). A cytosine was considered DMC if it showed at least a twofold change in methylation percentage in the mutant. The regions were then filtered to include only those with at least 10 DMCs and with at least a twofold change in arithmetic mean of methylation percentage of all cytosine.

For C24 data, clean reads were mapped to a pseudo-C24 genome using BRAT-BW allowing two mismatches. We used public data set of *ros1-1/nrpd1*(C24) double mutant in C24 background[41] to analyse type II RdDM targets. The pseudo-C24 genome was generated through the replacement of SNPs in the Col-0 genome with C24 variants (http://1001genomes.org/data/MPI/MPISchneeberger2011/releases/current//C24/Marker/C24.SNPs.TAIR9.txt).

TE border analysis. The analysis was according to previously described method[42]: *ros1-4* hyper-DMR associated TEs were aligned at the 5′ end or the 3′ end. We discarded from the analysis 250 bp from the end opposite to the one used for alignment to avoid averaging the edges of shorter TEs with the middles of longer sequences.

Histone feature analysis. Histone features were analysed according to a previously described method[4] with a minor modification: Briefly, the public data used for the analysis were downloaded from GEO (accession no. GSE28398)[36]. The reads were aligned to TAIR10 using Bowtie[43] allowing three mismatches. Only reads that were uniquely mapped to the genome were retained for the downstream analysis. To generate the relative histone signal distribution in the flanking 5 kb region of the mid-point of DMRs, the whole region (10,050 bp long) was divided into 201 bins with a size of 50 bp and the 101th bin aligning at the middle point of each DMR. The number of depth in each of the 201 bins was summed. The relative histone modification signal (y axis) in each of the 201 bins was defined as

$$n(\text{Histone\_modification}) \times N(\text{Input})/[N(\text{Histone\_modification}) \times n(\text{Input})]$$

where n is the sum of depth of the corresponding library in each bin and N is the number of mapped reads of the corresponding library.

For box plots, DMRs were considered as the 1050 bp region from the DMR mid-point (±10 bins plus the mid-bin). In each region, the relative histone modification signal was calculated as above. The box plots were generated in R using function 'boxplot' with parameter 'range = 1.5, outline = F, notch = T'. The *P*-values were calculated in R using function 'wilcox.test'.

Small RNA analysis. Small RNA samples were prepared from 14-day-old seedlings. The analysis pipeline was according to Zhang *et al.*[44].

Pol IV ChIP-seq analysis. The data sets we used are from a previously published paper[29]. According to this paper, the wild type is pure wild-type plants without any transgenes. *nrpd1/NRPD1-3×FLAG* is the *nrpd1* mutant with a *NRPD1-3×FLAG* transgene.

Data availability. The data discussed in this publication have been deposited in NCBI's Gene Expression Omnibus and are accessible through the GEO Series accession number GSE83802. Previously published data, including whole-genome sequencing data and ChIP-seq data, used in this study are listed in Supplementary Table 2.

Received 6 March 2016; accepted 3 October 2016; published 31 October 2016

References

1. Collier, J. Epigenetic regulation of the bacterial cell cycle. *Curr. Opin. Microbiol.* **12,** 722–729 (2009).
2. He, X.-J., Chen, T. & Zhu, J.-K. Regulation and function of DNA methylation in plants and animals. *Cell Res.* **21,** 442–465 (2011).
3. Zhu, J.-K. Active DNA demethylation mediated by DNA glycosylases. *Annu. Rev. Genet.* **43,** 143–166 (2009).
4. Yang, D.-L. *et al.* Dicer-independent RNA-directed DNA methylation in *Arabidopsis*. *Cell Res.* **26,** 66–82 (2016).
5. Zhai, J. *et al.* A one precursor one siRNA model for Pol IV-dependent siRNA biogenesis. *Cell* **163,** 445–455 (2015).
6. Ye, R. *et al.* A dicer-independent route for biogenesis of siRNAs that direct DNA methylation in *Arabidopsis*. *Mol. Cell* **61,** 222–235 (2016).
7. Blevins, T. *et al.* Identification of Pol IV and RDR2-dependent precursors of 24 nt siRNAs guiding *de novo* DNA methylation in *Arabidopsis*. *eLife* **4,** e09591 (2015).
8. Gong, Z. *et al.* ROS1, a repressor of transcriptional gene silencing in *Arabidopsis*, encodes a DNA glycosylase/lyase. *Cell* **111,** 803–814 (2002).
9. Agius, F., Kapoor, A. & Zhu, J.-K. Role of the *Arabidopsis* DNA glycosylase/lyase ROS1 in active DNA demethylation. *Proc. Natl Acad. Sci. USA* **103,** 11796–11801 (2006).
10. Morales-Ruiz, T. *et al.* DEMETER and REPRESSOR OF SILENCING 1 encode 5-methylcytosine DNA glycosylases. *Proc. Natl Acad. Sci. USA* **103,** 6853–6858 (2006).
11. Li, Y. *et al.* An AP endonuclease functions in active DNA demethylation and gene imprinting in *Arabidopsis* [corrected]. *PLoS Genet.* **11,** e1004905 (2015).
12. Martínez-Macías, M. I. *et al.* A DNA 3' phosphatase functions in active DNA demethylation in *Arabidopsis*. *Mol. Cell* **45,** 357–370 (2012).
13. Li, Y., Duan, C.-G., Zhu, X., Qian, W. & Zhu, J.-K. A DNA ligase required for active DNA demethylation and genomic imprinting in *Arabidopsis*. *Cell Res.* **25,** 757–760 (2015).
14. Qian, W. *et al.* A histone acetyltransferase regulates active DNA demethylation in *Arabidopsis*. *Science* **336,** 1445–1448 (2012).
15. Lang, Z. *et al.* The methyl-CpG-binding protein MBD7 facilitates active DNA demethylation to limit DNA hyper-methylation and transcriptional gene silencing. *Mol. Cell* **57,** 971–983 (2015).
16. Wang, C. *et al.* Methyl-CpG-binding domain protein MBD7 is required for active DNA demethylation in *Arabidopsis*. *Plant Physiol.* **167,** 905–914 (2015).
17. Zhu, J., Kapoor, A., Sridhar, V. V., Agius, F. & Zhu, J.-K. The DNA glycosylase/lyase ROS1 functions in pruning DNA methylation patterns in *Arabidopsis*. *Curr. Biol.* **17,** 54–59 (2007).
18. Yamamuro, C. *et al.* Overproduction of stomatal lineage cells in *Arabidopsis* mutants defective in active DNA demethylation. *Nat. Commun.* **5,** 4062 (2014).
19. Le, T.-N. *et al.* DNA demethylases target promoter transposable elements to positively regulate stress responsive genes in *Arabidopsis*. *Genome Biol.* **15,** 458 (2014).
20. Lister, R. *et al.* Highly integrated single-base resolution maps of the epigenome in *Arabidopsis*. *Cell* **133,** 523–536 (2008).
21. Zheng, X., Zhu, J., Kapoor, A. & Zhu, J.-K. Role of *Arabidopsis* AGO6 in siRNA accumulation, DNA methylation and transcriptional gene silencing. *EMBO J.* **26,** 1691–1701 (2007).
22. Penterman, J., Uzawa, R. & Fischer, R. L. Genetic interactions between DNA demethylation and methylation in *Arabidopsis*. *Plant Physiol.* **145,** 1549–1557 (2007).
23. Huettel, B. *et al.* Endogenous targets of RNA-directed DNA methylation and Pol IV in *Arabidopsis*. *EMBO J.* **25,** 2828–2836 (2006).
24. Lei, M. *et al.* Regulatory link between DNA methylation and active demethylation in *Arabidopsis*. *Proc. Natl Acad. Sci. USA* **112,** 3553–3557 (2015).
25. Williams, B. P., Pignatta, D., Henikoff, S. & Gehring, M. Methylation-sensitive expression of a DNA demethylase gene serves as an epigenetic rheostat. *PLoS Genet.* **11,** e1005142 (2015).
26. Penterman, J. *et al.* DNA demethylation in the *Arabidopsis* genome. *Proc. Natl Acad. Sci. USA* **104,** 6752–6757 (2007).
27. Matzke, M. A. & Mosher, R. A. RNA-directed DNA methylation: an epigenetic pathway of increasing complexity. *Nat. Rev. Genet.* **15,** 394–408 (2014).
28. Zhang, H. & Zhu, J.-K. Active DNA demethylation in plants and animals. *Cold Spring Harb. Symp. Quant. Biol.* **77,** 161–173 (2012).
29. Law, J. A. *et al.* Polymerase IV occupancy at RNA-directed DNA methylation sites requires SHH1. *Nature* **498,** 385–389 (2013).
30. Zemach, A. *et al.* The *Arabidopsis* nucleosome remodeler DDM1 allows DNA methyltransferases to access H1-containing heterochromatin. *Cell* **153,** 193–205 (2013).
31. He, X.-J. *et al.* A conserved transcriptional regulator is required for RNA-directed DNA methylation and plant development. *Genes Dev.* **23,** 2717–2722 (2009).
32. Gao, Z. *et al.* An RNA polymerase II- and AGO4-associated protein acts in RNA-directed DNA methylation. *Nature* **465,** 106–109 (2010).
33. Stroud, H. *et al.* Non-CG methylation patterns shape the epigenetic landscape in *Arabidopsis*. *Nat. Struct. Mol. Biol.* **21,** 64–72 (2014).
34. Mathieu, O., Reinders, J., Caikovski, M., Smathajitt, C. & Paszkowski, J. Transgenerational stability of the *Arabidopsis* epigenome is coordinated by CG methylation. *Cell* **130,** 851–862 (2007).
35. Eskandarian, H. A. *et al.* A role for SIRT2-dependent histone H3K18 deacetylation in bacterial infection. *Science* **341,** 1238858 (2013).
36. Luo, C. *et al.* Integrative analysis of chromatin states in *Arabidopsis* identified potential regulatory mechanisms for natural antisense transcript production. *Plant J.* **73,** 77–90 (2013).

37. Rose, C. M., van den Driesche, S., Meehan, R. R. & Drake, A. J. Epigenetic reprogramming: preparing the epigenome for the next generation. *Biochem. Soc. Trans.* **41,** 809–814 (2013).
38. Ponferrada-Marín, M. I., Martínez-Macías, M. I., Morales-Ruiz, T., Roldán-Arjona, T. & Ariza, R. R. Methylation-independent DNA binding modulates specificity of Repressor of Silencing 1 (ROS1) and facilitates demethylation in long substrates. *J. Biol. Chem.* **285,** 23032–23039 (2010).
39. Harris, E. Y., Ponts, N., Le Roch, K. G. & Lonardi, S. BRAT-BW: efficient and accurate mapping of bisulfite-treated reads. *Bioinformatics* **28,** 1795–1796 (2012).
40. Ausin, I. *et al.* INVOLVED IN DE NOVO 2-containing complex involved in RNA-directed DNA methylation in *Arabidopsis*. *Proc. Natl Acad. Sci. USA* **109,** 8374–8381 (2012).
41. Huang, C.-F. *et al.* A Pre-mRNA-splicing factor is required for RNA-directed DNA methylation in *Arabidopsis*. *PLoS Genet.* **9,** e1003779 (2013).
42. Ibarra, C. A. *et al.* Active DNA demethylation in plant companion cells reinforces transposon methylation in gametes. *Science* **337,** 1360–1364 (2012).
43. Langmead, B., Trapnell, C., Pop, M. & Salzberg, S. L. Ultrafast and memory-efficient alignment of short DNA sequences to the human genome. *Genome Biol.* **10,** R25 (2009).
44. Zhang, H. *et al.* An Rrp6-like protein positively regulates noncoding RNA levels and DNA methylation in *Arabidopsis*. *Mol. Cell* **54,** 418–430 (2014).

Acknowledgements

This work was supported by National Institutes of Health Grant R01GM070795 and by the Chinese Academy of Sciences (to J.-K. Z.).

Author contributions

J.-K.Z, Z.L. and K.T. designed the study, interpreted the data and wrote the manuscript. K.T. and Z.L. did the bioinformatics analysis. H.Z. performed sequencing experiments.

Additional information

Supplementary information is available for this paper. Reprints and permissions information is available at www.nature.com/reprints. Correspondence and requests for materials should be addressed to Z.L.

Competing interests

The authors declare no competing financial interests.